 doi:10.20944/preprints202101.0333.v1

Article

Synthesis and Deposition of Thermochromic VO_2 Thin Films from Peroxide-based Chemical Solutions

Matthias Van Zele[1], Hannes Rijckaert[1] , Davy Deduytsche[2], Christophe Detavernier[2], Isabel Van Driessche[1], Dirk Poelman[3] and Klaartje De Buysser [1,*]

[1] Ghent University, Department of Chemistry, SCRiPTS, Krijgslaan 281-S3, 9000 Ghent, Belgium; Matthias.VanZele@ugent.be (M.V.Z.); Hannes.Rijckaert@ugent.be (H.R.); Isabel.VanDriessche@ugent.be (I.V.D.); Klaartje.DeBuysser@ugent.be (K.D.B.)

[2] Ghent University, Department of Solid State Sciences, CoCooN, Krijgslaan 281-S1, 9000 Ghent, Belgium; Davy.Deduytsche@ugent.be (D.D.); Christophe.Detavernier@ugent.be (C.D.)

[3] Ghent University, Department of Solid State Sciences, LumiLab, Krijgslaan 281-S1, 9000 Ghent, Belgium; Dirk.Poelman@ugent.be (D.P.)

* Correspondence: Klaartje.DeBuysser@ugent.be; Tel.: +32-9-264-4441

Abstract: In this paper, a novel synthesis for a chemical precursor for nanocrystalline VO_2 coatings is elaborated. The compatibility of the precursor towards the substrate is optimized for spin coating. This is done by subjecting multiple solvents to contact angle measurements. A suitable thermal treatment is developed to densify the coating and to induce crystallization. Afterwards the microstructure of the coating is investigated using X-Ray diffraction, electron microscopy and ellipsometry techniques. To assess the thermochromic properties of the fabricated device, optical transmission experiments were conducted both at room temperature and at elevated temperature. A correlation between these thermochromic properties and coating thickness was investigated in order to obtain an optimized thermochromic device, where both high visual transparency and prominent thermochromic switching abilities are aimed for. In this work, an optimal coating thickness is proposed for a thermochromic coating with high switching ability and solar modulation.

Keywords: Wet chemical deposition; crystalline thin films; vanadium dioxide; thermochromism

1. Introduction

Vanadium dioxide (VO_2) is a promising smart material which undergoes a reversible thermochromic transition at a critical temperature T_c of 68 °C. Below this transition temperature, the material resides in a monoclinic crystal structure and is transparent to mid- and far-infrared (IR) radiation. Above the critical temperature, the crystal structure shifts towards a rutile structure and the material shows reflective properties for mid- and far-IR radiation [1–3]. These optical properties render the material of great interest for glazing devices, which are able to shift the insulating properties in a reversible way, depending on the external temperature [4–7].

This reversible transition is often referred to as the thermochromic effect or the metal-to-insulator transition, as there is also a shift in electronic properties, which causes the material to switch from an insulator to a metallic state. This is due to the rearrangement of vanadium ions when shifting between the monoclinic and the rutile crystal structures. In the monoclinic structure, the 3d orbitals of neighboring vanadium ions overlap, splitting this $d_{//}$ band in a bonding and antibonding combination in the orbital diagram (Figure 1). As a consequence, the Fermi level is situated between the conduction band and the valence band, typically resulting in an insulating material. In the rutile crystal phase however, the overlap between the 3d orbitals of neighbouring vanadium ions is no longer present and the $d_{//}$ band remains non-bonding. In contrast to the insulating state, the Fermi level is now situated in this non-bonding $d_{//}$ band, thus the material gains metallic properties.

Preprints (www.preprints.org) | NOT PEER-REVIEWED | Posted: 18 January 2021 doi:10.20944/preprints202101.0333.v1

To produce VO_2 based coatings, two general approaches can be followed. The first method consists of the synthesis of preformed VO_2(M) particles, followed by a deposition step in a suitable matrix [8–13]. According to both the Maxwell-Garnett effective-medium theory and the four-flux method, particle sizes should not exceed 20 nm to avoid scattering effects [14]. This is challenging, as literature of VO_2 particle based coatings reports particle sizes above 30 nm [15] up to several hundreds of nanometers [13,16] or even sizes in the micrometer range [10,17]. As the size of preformed VO_2 particles is very hard to control, subsequently the production of visibly transparent thermochromic devices is burdensome.

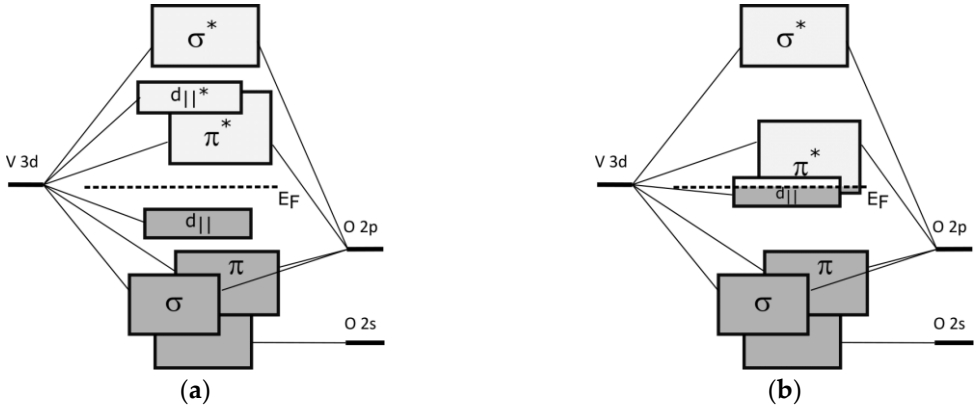

Figure 1: Comparison between the molecular orbital diagrams of the (a) low-temperature insulator state and the (b) high-temperature metallic state. In the insulator state, the $d_{||}$ orbitals are split up in a bonding and anti-bonding state due to efficient overlap of these orbitals between neighboring vanadium ions. Also the π^* orbitals are raised in energy due to orthorhombic distortion. In the metallic state, orthorhombic distortion is no longer present, lowering the energy of the π^* orbitals. Due to the impossibility of an efficient overlap of the $d_{||}$ orbitals, these remain nonbonding.

Another approach is first to formulate a chemical precursor solution, which can be deposited on the substrate by means of chemical solution deposition. Following this deposition step, a thermal treatment is conducted on the coated substrate to induce crystallization of the deposited material. Over the last years, the chemical solution deposition (CSD) method has gained a lot of interest due to its low cost and easy scalability with high efficiency [18]. In contrast to the preformed particles route, this approach can be optimized towards continuous production methods such as roll-to-roll, ink-jet or slot-die coating. Preceding literature has already given valuable insight in physical deposition methods [19–22]. However, procedures reporting chemical solution deposition methods are limited, making use of polymer-assisted methods or sol-gel methods to deposit VO_2 layers on preformed particles [23].

In this work, a suitable precursor formulation was developed towards optimal compatibility with the substrate. To obtain this, the choice of solvent was adjusted. A suitable coating method was searched for to obtain optimal coating thickness. The influence of the amount of coating runs on the thermochromic properties was investigated. The obtained coating's microstructure was fully investigated by a variety of characterization methods. Subsequently, the thermochromic properties were assessed and correlated to the coating microstructure and thickness.

2. Materials and Methods

2.1 Precursor formulation and characterization

The VO_2 precursor solution was prepared by adding 0.028 g of V_2O_5 powder (Sigma-Aldrich) to 3.8 mL of water or 1-butanol (Sigma-Aldrich). Subsequently, 0.2 mL of 30% H_2O_2 (w/w) in H_2O solution was added and the mixture was magnetically stirred for 30 minutes. The color shifted from a yellow

Preprints (www.preprints.org) | NOT PEER-REVIEWED | Posted: 18 January 2021 doi:10.20944/preprints202101.0333.v1

suspension to a deep-red solution, indicating that vanadium diperoxo $[VO(O_2)_2]^-$ complex was formed [24–26].

Contact angle measurements were conducted with a Drop Shape Analyzer DSA30 (Krüss GmbH, Hamburg, Germany). The contact angles were measured using 0.5 µL droplets.

2.2 Thin film deposition and thermal treatment

Quartz substrates (Structure Probe inc., West Chester PA, USA) were cleaned by ultrasonification in isopropanol (Acros organics) for 1 hour. Before deposition, the substrates were dried by heating on a hot-plate at 120 °C. Next, 45 µL of the VO_2 precursor solution was dropped on the substrate for spin coating (SCC-200 SpinCoater, Schaefer Technologie GmbH, Langen, Germany). The substrate was spun at 1500 rpm for 30 seconds. After coating, the wet coating was dried on a hot-plate at 120 °C for 1 minute. While samples A and B both were coated one time, samples C and D were subject to an additional coating run.

Subsequently, the deposited films were thermally treated in a tube furnace under inert nitrogen atmosphere with a flow of 0.35 mL/min. The furnace was heated to 700 °C at a rate of 10 °C/min. This temperature was held for 1 hour, after which the furnace was cooled down naturally.

2.3 Thin film characterization

In-situ XRD measurements were carried out on a Bruker D8 Discover XRD system equipped with a Cu X-ray source (λ = 1.5406 Å) and a linear X-ray detector. The samples were put on a Si sample holder which was heated in a nitrogen atmosphere at a heating rate of 5°C/min. While heating every 15s an XRD spectrum was collected.

The microstructure was studied with a JEOL JEM 2200-FS scanning transmission electron microscopy (STEM) operated at 200 kV with high-angle annular dark-field (HAADF) detector. Samples for HAADF- STEM were prepared by cutting cross-sectional lamellae via focused ion beam technique in a FEI Nova 600 Nanolab Dual Beam scanning electron microscopy. The lamella were extracted using the *in-situ* lift-out procedure with an Omniprobe extraction needle. Prior to lamella preparation, an additional gold layer was sputtered on the samples to protect them. Compositional information was observed via combining HAADF-STEM with energy dispersive x-ray spectroscopy (EDX) mapping.

Optical transmission measurements in the wavelength range 250 nm – 2500 nm were performed using a Perkin Elmer Lambda L1050 spectrophotometer. A Linkam TMS600 hot stage was mounted in the sample compartment to allow temperature dependent measurements, and a Spectralon coated 150 mm integrating sphere with PMT and InGaAs detectors was used to collect the light.

Spectroscopic ellipsometry measurements were carried out with a J. A. Woollam M-2000 ellipsometer working in the ultraviolet to visible region. Measurements were performed with an acquisition time of 5 s. Data analysis was carried out using the CompleteEase software package (version 6.34).

IR switching is defined as the difference in transmittance between 25 °C and 100 °C, measured at λ = 2000 nm.

$$\Delta T_{IR}(\%) = T_{IR}(25°C) - T_{IR}(100°C), \quad (1)$$

The solar modulation is calculated as:

$$T_{sol} = \frac{\int \varphi_{sol}(\lambda) T(\lambda) d\lambda}{\int \varphi_{sol}(\lambda) d\lambda}, \quad (2)$$

$$\Delta T_{sol} = \Delta T_{sol(25°C)} - \Delta T_{sol(100°C)}, \quad (3)$$

where φ is the solar (sol) irradiance spectrum for air mass 1.5 corresponding to the sun standing 37° above the horizon [27]. The critical temperature T_c was calculated by identifying the transition temperature during heating (T_1) and cooling (T_2) and using equation 4. Following, the width of the hysteresis ΔT_c loop was calculated (equation 5).

Preprints (www.preprints.org) | NOT PEER-REVIEWED | Posted: 18 January 2021 doi:10.20944/preprints202101.0333.v1

$$T_c = \frac{T_1+T_2}{2}, \quad (4)$$

$$\Delta T_c = T_1 - T_2, \quad (5)$$

3. Results and Discussion

3.1. Precursor optimazation

To obtain a precursor formulation which is suitable for spin coating, a good wetting behavior of the precursor on the substrate should be guaranteed. Contact angle measurements were therefore conducted to assess the compatibility between the chemical precursor and the quartz substrate, where a good wetting is manifested as low contact angles between the liquid chemical precursor and the solid substrate.

As can be seen in figure 2, a relatively high contact angle of 60.50 ± 0.47° is measured when using water as solvent for the chemical precursor by using the tangent method. Spin coating of this type of precursor is not feasible to fabricate uniform coatings. However, when using 1-butanol as solvent, a contact angle of only 7.60 ± 2.15° is measured with circle fitting. This shows an improved affinity between the chemical precursor and the substrate when compared to the water-based chemical precursor solution. Consequently, further deposition steps were conducted using the 1-butanol-based precursor.

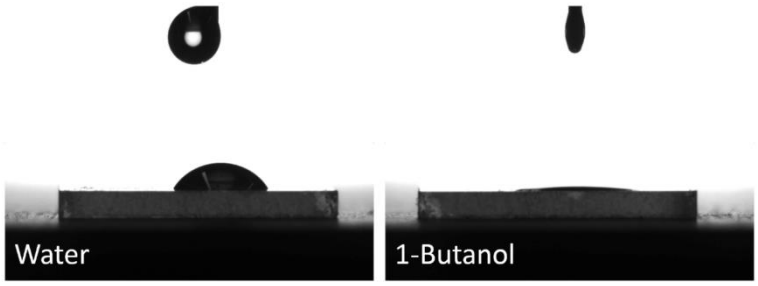

Figure 2. Images taken during contact angle measurements of the chemical precursor in water and 1-butanol.

3.2. Structural characterization of VO_2 coating

To densify and to induce crystallization of the deposited material, a thermal treatment in inert atmosphere is necessary. To assess the crystallinity and to have a first confirmation that indeed monoclinic VO_2 was formed during the thermal process, the coated substrate was heated to induce the thermochromic switching, while the crystal structure was monitored via *in-situ* XRD.

As can be seen in the *in-situ* XRD patterns (Figure 3), the (011) reflection ($2\theta = 27.8°$) of monoclinic VO_2 is recorded below the critical temperature. Above the critical temperature, this reflection fades out, while the (110) reflection ($2\theta = 27.6°$) of rutile VO_2 is recorded. It should be noted that the critical temperature of this system shifted towards a higher temperature than the intrinsic 68 °C and even higher than the calculated critical temperature, discussed in the following section. This is due to the relatively high thermal mass of the quartz substrate, causing a difference between the expected temperature of the substrate and the programmed furnace temperature in the *in-situ* XRD setup.

Preprints (www.preprints.org) | NOT PEER-REVIEWED | Posted: 18 January 2021 doi:10.20944/preprints202101.0333.v1

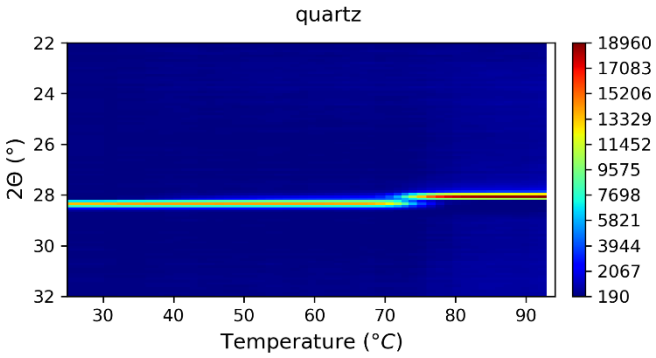

Figure 3. *In-situ* XRD pattern of a coated substrate, measured from 25 °C to 100 °C. The color scale depicts the intensity of the signal in arbitrary units.

HAADF-STEM measurements were used to assess the thickness of the formed VO_2 thin layers. For this, STEM lamella were prepared via FIB, of which compositional information was gathered via EDX mapping. Figure 4 shows where Au, V and Si were detected on the STEM lamella. The quartz substrate can easily be identified as the region where only Si is detected. However, positioning a clear boundary between vanadium and the sputtered gold layer on top, is not straightforward. As can be seen in the overlay picture, gold and vanadium are intermixed on top of the quartz substrate. This is possible due to the sputtering process of the gold layer, partially destroying the VO_2 thin film. The bottom part of Figure 4 shows the obtained EDX profile. While the intensity is low, it is clearly visible that vanadium is intermixed with the sputtered gold. As the vanadium signal was significantly lower than the silicon and gold signals, no decisive conclusion on the thickness of the VO_2 thin film could be drawn from this experiment.

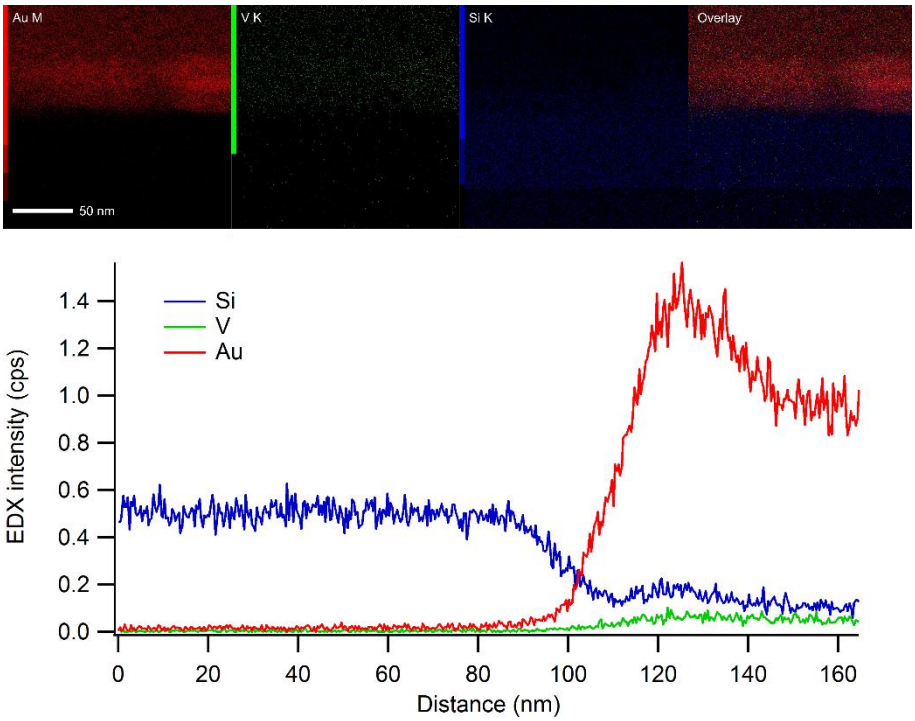

Figure 4. (top) EDX mapping and (bottom) EDX profile of the deposited coating and the underlying quartz substrate. The overlay picture show mixing of the deposited VO_2 thin film and gold. The latter was deposited for improved conductivity, necessary for FIB preparation of TEM lamella.

Due to this phenomenon, an additional characterization technique is necessary to obtain thickness information. Ellipsometry was thus used to determine the thicknesses of the top VO_2

Preprints (www.preprints.org) | NOT PEER-REVIEWED | Posted: 18 January 2021 doi:10.20944/preprints202101.0333.v1

coating. Figure 5 shows a representative ellipsometry measurement, where a Tauc-Lorentz model was fitted to both the measured Psi and Delta values. An overview of the obtained thicknesses using this technique is shown in Table 1. According to the results obtained, single coatings yield a thin film thickness around 35 nm, while double coatings show a thin film thickness of 45 nm.

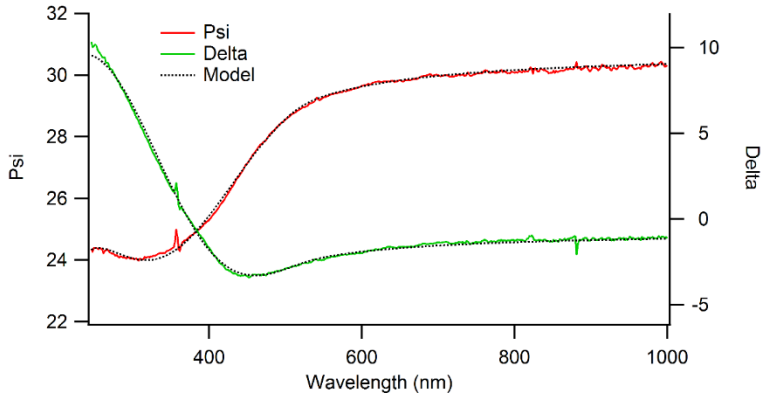

Figure 5. Typical ellipsometry measurement of the coated substrates. The dotted traces represent the fitted models for both the measured Ψ and Δ.

Table 1. Relation between number of coating runs and the thickness obtained via ellipsometry.

Sample code	Coating runs (number)	Thickness (nm)
A	1	34.32
B	1	35.06
C	2	44.09
D	2	45.31

The increase in coating thickness is not linear. This is possibly due to the fact that the primary deposited coating was not dry completely or due to redissolution of this coating upon deposition of the second layer. A possible approach to obtain thicker coatings is to perform an intermediate thermal treatment between each deposition step. However, this is out of scope of this work, as the aim is to obtain coatings with a high visual transparency.

3.2. Thermochromic properties

To assess the thermochromic properties of the deposited VO_2 coating, optical transmission measurements were conducted both at elevated (100 °C) and at room temperature. Figure 6 shows an overview of the obtained transmission spectra of the coated substrates, depicted in Table 2. The thinner coatings (spectra A and B) show a high transparency in the infrared region between 1000 nm and 2500 nm at room temperature (blue trace). For the spectra recorded at 100 °C, the transmission in the infrared region is lowered drastically. This indicates that the VO_2 coating indeed shows thermochromic properties.

Comparing these findings to the spectra of the thicker coatings (spectra C and D), it is noted that the transmittance increases again in the region between 2000 nm and 2500 nm. This can be due to microstructural effects and defects that were induced during the thermal process [28]. Additional to this, the spectra show a clear minimum around 1350 nm. This corresponds to the surface plasmon absorption of metallic VO_2 (R) [8,29].

When comparing the spectra in general, the thinner coatings (A and B) show higher IR switching numbers than the thicker coatings (C and D). The IR switching values are summarized in Table 2.

Preprints (www.preprints.org) | NOT PEER-REVIEWED | Posted: 18 January 2021 doi:10.20944/preprints202101.0333.v1

Table 2. Summary of the thermochromic properties for each sample.

Sample code	IR switching ΔT_{IR} (%)	Solar modulation ΔT_{sol} (%)	Hysteresis ΔT_c (°C)	Critical temperature T_c (°C)
A	8.03	3.05	13	71.3
B	6.31	3.43	24	74.5
C	0.98	2.54	44	56.3
D	1.62	2.83	44	59.0

[1] Tables may have a footer

The thinner coatings clearly show a high IR switching ability with fairly narrow hysteresis widths. The solar modulation resides around 3%, which is to be expected for nanosized VO_2 layers [30,31].

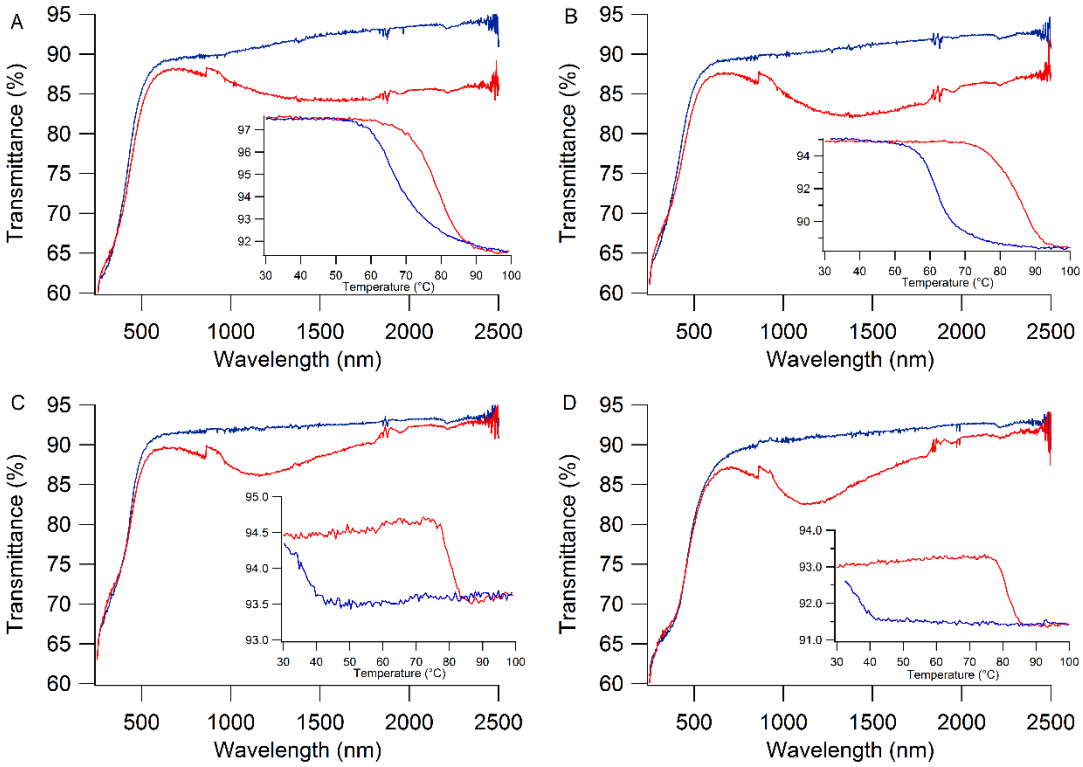

Figure 6. Optical measurements of the coated substrate at both room temperature (blue trace) and 100 °C (red trace). The insets show the respective hysteresis curve, recorded at 2000 nm, of the thermochromic device.

As can be seen in Figure 6; an optimum in balance between visual transparency and thermochromic properties has to be aimed for. The thinner coatings have a higher IR switching ability and narrow hysteresis. According to the hysteresis plots, the transition is more prominent for the thinner coatings. Therefore, a coating thickness in the range of 35 nm should be aimed for to obtain optimal properties.

4. Conclusions

The main conclusion of this work is that a suitable chemical precursor for the deposition of thermochromically active VO_2 layers was developed. The chemical precursor consisted of commercially available V_2O_5 powder modified with H_2O_2. The use of 1-butanol as solvent of choice gave rise to optimal compatibility with the used quartz substrates. Using straightforward spin-coating methods, the chemical precursor was deposited on these substrates. Subsequently, a simple thermal process in inert nitrogen atmosphere was conducted to induce crystallization of the

deposited material towards monoclinic VO_2 thin layers. Layer thicknesses were determined by ellipsometry, as electron microscopic measurements seemed unsuitable due to the use of quartz substrates.

After one coating run, layers with thicknesses of 35 nm were deposited with a high IR switching power over 6% and fairly narrow hysteresis widths. Multiple deposition runs led to thicker VO_2 layers, however with a considerably high contribution of plasmonic resonance effects [8,29].

This work shows that it is possible to deposit crystalline and thermochromically active VO_2 layers on quartz substrates in a straightforward process, producing thermochromic coatings with high IR switching numbers. An optimal coating thickness is proposed to be 35 nm, where both high visual transparency and high thermochromic switching is achieved.

Author Contributions: M.V.Z. and K.D.B. conceived and designed the experiments; H.R. made TEM lamella and carried EDX measurements out; D.D. and C.D. performed ellipsometry measurements; D.P. made the optical measurements; I.V.D and K.D.B. provided supervision. All authors have read and agreed to the published version of the manuscript.

Funding: This research received no external funding.

Conflicts of Interest: The authors declare no conflict of interest.

References

1. Goodenough, J.B. The two components of the crystallographic transition in VO2. *J. Solid State Chem.* **1971**, *3*, 490–500.
2. Haverkort, M.W.; Hu, Z.; Tanaka, A.; Reichelt, W.; Streltsov, S. V; Korotin, M.A.; Anisimov, V.I.; Hsieh, H.H.; Lin, H.J.; Chen, C.T.; et al. Orbital-assisted metal-insulator transition in VO2. *Phys. Rev. Lett.* **2005**, *95*.
3. Eyert, V. The metal-insulator transitions of VO2: A band theoretical approach. *Ann. der Phys.* **2002**, *11*, 650–702.
4. Wang, S.; Liu, M.; Kong, L.; Long, Y.; Jiang, X.; Yu, A. Recent progress in VO2 smart coatings: Strategies to improve the thermochromic properties. *Prog. Mater. Sci.* 2016.
5. Seyfouri, M.M.; Binions, R. Sol-gel approaches to thermochromic vanadium dioxide coating for smart glazing application. *Sol. Energy Mater. Sol. Cells* **2017**, *159*, 52–65.
6. Gonçalves, A.; Resende, J.; Marques, A.C.; Pinto, J. V.; Nunes, D.; Marie, A.; Goncalves, R.; Pereira, L.; Martins, R.; Fortunato, E. Smart optically active VO2 nanostructured layers applied in roof-type ceramic tiles for energy efficiency. *Sol. Energy Mater. Sol. Cells* **2016**, *150*, 1–9.
7. Xu, F.; Cao, X.; Luo, H.; Jin, P. Recent advances in VO2-based thermochromic composites for smart windows. *J. Mater. Chem. C* **2018**, *6*, 1903–1919.
8. Guo, D.; Ling, C.; Wang, C.; Wang, D.; Li, J.; Zhao, Z.; Wang, Z.; Zhao, Y.; Zhang, J.; Jin, H. Hydrothermal One-Step Synthesis of Highly Dispersed M-Phase VO2 Nanocrystals and Application to Flexible Thermochromic Film. *ACS Appl. Mater. Interfaces* **2018**, *10*, 28627–28634.
9. Chen, Z.; Gao, Y.; Kang, L.; Cao, C.; Chen, S.; Luo, H. Fine crystalline VO2 nanoparticles: Synthesis, abnormal phase transition temperatures and excellent optical properties of a derived VO 2 nanocomposite foil. *J. Mater. Chem. A* **2014**, *2*, 2718–2727.
10. Madida, I.G.; Simo, A.; Sone, B.; Maity, A.; Kana Kana, J.B.; Gibaud, A.; Merad, G.; Thema, F.T.; Maaza, M. Submicronic VO2-PVP composites coatings for smart windows applications and solar heat management. *Sol. Energy* **2014**, *107*, 758–769.
11. Li, M.; Magdassi, S.; Gao, Y.; Long, Y. Hydrothermal Synthesis of VO2 Polymorphs: Advantages, Challenges and Prospects for the Application of Energy Efficient Smart Windows. *Small* 2017, *13*, 1701147.

12. Janamphansang, L.; Wootthikanokkhan, J.; Nawalertpanya, S. Preparation of VO2 nanoparticles with surface functionalization for thermochromic application. *Eng. J.* **2019**, *23*, 205–215.
13. Zomaya, D.; Xu, W.Z.; Grohe, B.; Mittler, S.; Charpentier, P.A. W-doped VO2/PVP coatings with enhanced thermochromic performance. *Sol. Energy Mater. Sol. Cells* **2019**, *200*, 109900.
14. Laaksonen, K.; Li, S.Y.; Puisto, S.R.; Rostedt, N.K.J.; Ala-Nissila, T.; Granqvist, C.G.; Nieminen, R.M.; Niklasson, G.A. Nanoparticles of TiO2 and VO2 in dielectric media: Conditions for low optical scattering, and comparison between effective medium and four-flux theories. *Sol. Energy Mater. Sol. Cells* **2014**, *130*, 132–137.
15. Kim, Y.; Yu, S.; Park, J.; Yoon, D.; Dayaghi, A.M.; Kim, K.J.; Ahn, J.S.; Son, J. High-throughput roll-to-roll fabrication of flexible thermochromic coatings for smart windows with VO2 nanoparticles. *J. Mater. Chem. C* **2018**, *6*, 3451–3458.
16. Xygkis, M.; Gagaoudakis, E.; Zouridi, L.; Markaki, O.; Aperathitis, E.; Chrissopoulou, K.; Kiriakidis, G.; Binas, V. Thermochromic behavior of VO 2 /polymer nanocomposites for energy saving coatings. *Coatings* **2019**, *9*, 163.
17. Gonçalves, A.; Resende, J.; Marques, A.C.; Pinto, J. V.; Nunes, D.; Marie, A.; Goncalves, R.; Pereira, L.; Martins, R.; Fortunato, E. Smart optically active \ce{VO2} nanostructured layers applied in roof-type ceramic tiles for energy efficiency. *Sol. Energy Mater. Sol. Cells* **2016**, *150*, 1–9.
18. Rijckaert, H.; Cayado, P.; Nast, R.; Diez Sierra, J.; Erbe, M.; López Dominguez, P.; Hänisch, J.; De Buysser, K.; Holzapfel, B.; Van Driessche, I. Superconducting HfO2-YBa2Cu3O7−δ Nanocomposite Films Deposited Using Ink-Jet Printing of Colloidal Solutions. *Coatings* **2019**, *10*, 17.
19. Blackman, C.S.; Piccirillo, C.; Binions, R.; Parkin, I.P. Atmospheric pressure chemical vapour deposition of thermochromic tungsten doped vanadium dioxide thin films for use in architectural glazing. *Thin Solid Films* **2009**, *517*, 4565–4570.
20. Wilkinson, M.; Kafizas, A.; Bawaked, S.M.; Obaid, A.Y.; Al-Thabaiti, S.A.; Basahel, S.N.; Carmalt, C.J.; Parkin, I.P. Combinatorial atmospheric pressure chemical vapor deposition of graded TiO2-VO2 mixed-phase composites and their dual functional property as self-cleaning and photochromic window coatings. *ACS Comb. Sci.* **2013**, *15*, 309–319.
21. Bahlawane, N.; Lenoble, D. Vanadium Oxide Compounds **:** Structure, Properties, and Growth from the Gas Phase. *Chem. Vap. Depos.* **2014**, *20*, 299–311.
22. Chiu, T.W.; Tonooka, K.; Kikuchi, N. Growth of b-axis oriented VO 2 thin films on glass substrates using ZnO buffer layer. *Appl. Surf. Sci.* **2010**, *256*, 6834–6837.
23. Gao, Y.; Luo, H.; Zhang, Z.; Kang, L.; Chen, Z.; Du, J.; Kanehira, M.; Cao, C. Nanoceramic VO 2 thermochromic smart glass: A review on progress in solution processing. *Nano Energy* 2012, *1*, 221–246.
24. Nguyen, T.D.; Do, T.O. Solvo-hydrothermal approach for the shape-selective synthesis of vanadium oxide nanocrystals and their characterization. *Langmuir* **2009**, *25*, 5322–5332.
25. Yu, L.; Zhang, X. Hydrothermal synthesis and characterization of vanadium oxide/titanate composite nanorods. *Mater. Chem. Phys.* **2004**, *87*, 168–172.
26. Alonso, B.; Livage, J. Synthesis of Vanadium Oxide Gels from Peroxovanadic Acid Solutions: A 51V NMR Study. *J. Solid State Chem.* **1999**, *148*, 16–19.
27. American Society for Testing and Materials G173-03: Standard tables for reference solar spectral irradiances: direct normal and hemispherical on 37° tilted surface. *ASTM* 2012.
28. Minch, R.; Moonoosawmy, K.R.; Solterbeck, C.H.; Es-Souni, M. The influence of processing conditions on the morphology and thermochromic properties of vanadium oxide films. *Thin Solid Films* **2014**, *556*,

 doi:10.20944/preprints202101.0333.v1

277–284.

29. Li, S.Y.; Niklasson, G.A.; Granqvist, C.G. Nanothermochromics: Calculations for VO2 nanoparticles in dielectric hosts show much improved luminous transmittance and solar energy transmittance modulation. *J. Appl. Phys.* **2010**, *108*, 063525.
30. Li, R.; Ji, S.; Li, Y.; Gao, Y.; Luo, H.; Jin, P. Synthesis and characterization of plate-like VO2(M)@SiO 2 nanoparticles and their application to smart window. *Mater. Lett.* **2013**, *110*, 241–244.
31. Chen, S.; Dai, L.; Liu, J.; Gao, Y.; Liu, X.; Chen, Z.; Zhou, J.; Cao, C.; Han, P.; Luo, H.; et al. The visible transmittance and solar modulation ability of VO2 flexible foils simultaneously improved by Ti doping: An optimization and first principle study. *Phys. Chem. Chem. Phys.* **2013**, *15*, 17537–17543.